

Microfluidic-based synthesis of non-spherical magnetic hydrogel microparticles†

Dae Kun Hwang, Dhananjay Dendukuri and Patrick S. Doyle*

Received 27th March 2008, Accepted 3rd June 2008

First published as an Advance Article on the web 6th August 2008

DOI: 10.1039/b805176c

Spherical and non-spherical magnetic hydrogel particles were synthesized in a microfluidic device containing an embedded UV light reflector. Monodisperse magnetic emulsion droplets were generated in a T-junction and allowed to relax into spheres, disks, and plugs in confining microchannel geometries. Particle morphology was locked-in *via* UV-initiated photopolymerization. The role of the reflector in the microchannel is to provide a uniform distribution of UV energy to the magnetic emulsion droplets and to increase the UV flux, which significantly improves UV polymerization conditions for microfluidic-based particle synthesis. Magnetic nanoparticles were uniformly encapsulated in the hydrogel, giving the microparticles superparamagnetic behavior. Additionally, the non-spherical particles show anisotropic responses under an applied external magnetic field.

1 Introduction

The ability to fabricate large quantities of uniform particles with a large diversity of customizable morphologies and physicochemical properties would be a great asset to many advanced applications. Functional composite particles created through the incorporation of an inorganic material into a polymer network provide great potential in a broad range of applications such as cosmetics,¹ optics,^{2,3} and biotechnology.^{4,5} In particular, microparticles consisting of magnetic nanoparticles encapsulated in a polymer matrix are of great interest in biomedical applications for drug delivery,⁶ image enhancement,⁷ hyperthermia,⁸ sorting and separation,⁹ and immunoassays¹⁰ due to simple and controllable manipulations by an external stimulus.⁴ For practical use, monodisperse composite microparticles with homogeneous morphologies are highly desirable due to their consistent and reproducible behavior. For biomedical applications, biocompatibility and biodegradability are also essential for the particles. Various heterophase polymerization methods including macro-/mini-/microemulsion and suspension polymerization have been developed and implemented to synthesize both polymeric and composite particles.^{11–13} These batch polymerization methods do not offer control over particle morphology and have been used to primarily generate spherical particles. Non-spherical shapes, however, are highly desired for their properties such as anisotropic responses to external fields, large surface areas, and unique structure formation.¹⁴ Using bulk methods, it is also difficult to achieve a homogenous distribution of inorganic particles within a polymer matrix, especially magnetic particles in microgels.^{15,16}

Much effort has been devoted to generating particles with various morphologies based on either the controlled growth and nucleation of molecular species during precipitation^{17,18} or the template-assisted manipulation of spherical particles.^{19,20} The former technique imposes limitations on size and shape, while the latter is less flexible in shape selection due to the template dependence and the extra step required for the initial particle generation. More complex, non-spherical 2D and 3D particle shapes have been synthesized using photolithography,²¹ non-wetting template molding,²² stretching of spherical particles,²³ and seed emulsion polymerization.^{14,24} These studies, however, have mostly concentrated on homogenous polymeric particles, not composite particles.

Microfluidic devices present an alternative technique for the generation of monodisperse emulsion droplets by coflowing two immiscible fluids to induce drop formation.²⁵ The size of monodisperse emulsion droplets may be controlled by simply tuning the relative flow rates of the two fluids.^{26–29} In these devices, spherical emulsion droplets are usually generated since the disperse phase seeks to minimize its interfacial free energy. However, if the droplet radius is significantly larger than the smallest dimension of the channel it will be confined into a disk, plug, or rod.^{30,31} Ultraviolet (UV) and thermal energy are commonly used to solidify spherical and non-spherical droplets carrying either a UV- or thermal-curable polymer. Many groups have successfully synthesized spherical and/or non-spherical microgels,³² polymeric particles^{30,31,33–36} and composite particles.^{3,31,37} UV-initiated photopolymerization of particles in microfluidic devices is generally preferred due to the rapid polymerization kinetics. Furthermore, fast polymerization is essential to preserve internal structural uniformity and patterns incorporated in composites. For example, with slow polymerization kinetics, a liquid crystal mixed with a polymer will aggregate.³¹ Traditional polymerization schemes in microfluidic devices fail for composites consisting of inorganic materials because polymerization is slowed due to strong UV absorption

Department of Chemical Engineering, Massachusetts Institute of Technology, 77 Massachusetts Ave, Cambridge 02139, MA, USA. E-mail: pdoyle@mit.edu

† Electronic supplementary information (ESI) available: Table S1, magnetic properties of spherical microparticles. See DOI: 10.1039/b805176c

by the opaque inorganic material. This results in shape deformation or failure of the internal uniformity. Thus, the controlled synthesis of magnetic microparticles using microfluidics has not been greatly explored. To our knowledge, only one recent study has been reported in which a microfluidic device was used to produce magnetic spheres *via* a redox reaction.³⁷ However, the magnetic properties of the particles were not reported and aggregation of the magnetic nanoparticles was observed.

Here, we introduce the simple and controlled synthesis of magnetic microhydrogels using a conventional T-junction microfluidic device in combination with a UV light reflector, which dramatically improves the polymerization conditions for microfluidic-based particle synthesis. The method provides magnetic microhydrogels that are monodisperse, have a homogenous distribution of magnetic nanoparticles within the hydrogels, and can be tuned for the synthesis of non-spherical particles.

2 Experiment

2.1 Microfluidic devices

Rectangular microfluidic channels were fabricated using soft lithography by pouring poly-dimethylsiloxane (PDMS, Sylgard 184, Dow Corning) on a positive-relief silicon wafer patterned with SU-8 photoresist (Microchem). A small piece of aluminium foil, acting as a UV light reflector, was inserted into the liquid PDMS mixture and arranged at the target area of the patterned wafer with a thin layer of PDMS remaining between the aluminium reflector and the microchannels. The PDMS microchannels were sealed by bonding the PDMS layer patterned with the channels to a PDMS coated glass sheet using a PDG-32G plasma sterilizer (Harrick). The PDMS microfluidic

devices were then baked at 393 K for 2 h in order to render surfaces of the channels hydrophobic.³⁸ Fig. 1 shows a schematic diagram of a PDMS microfluidic device and its dimensions. For the synthesis of spherical microhydrogels, a stepped-height PDMS channel was used with dimensions of height (h) = 16 μm /width (w) = 40 μm in the T-junction and h = 75 μm / w = 200 μm downstream where the drop relaxes to a spherical shape. For disks, the dimensions were h = 40 μm / w = 40 μm in the T-junction and h = 40 μm / w = 80 μm downstream. For plugs, the dimensions were h = 16 μm / w = 40 μm for both the T-junction and downstream region. The droplets were exposed to UV light in the downstream region where the UV light reflector is present.

2.2 Materials

Magnetic nanoparticles ($\gamma\text{-Fe}_2\text{O}_3$) were synthesized based on Massart's method.³⁹ A mixture of 40 ml of Fe^{III} (1 M) and 10 ml of Fe^{II} (2 M) in an acidic medium (HCl) was slowly added to a solution of 400 ml (0.75M NaOH) while stirring and maintaining the solution at 373 K. The mixture was kept at 373 K for additional 10 min. After a magnetic decantation, the red precipitate was dispersed in 300 ml of distilled water and then 11.5 g of sodium citrate was added. The mixture was heated for 363 K for 30 min. A final 10% (w/v) concentration of the ferrofluid was obtained in distilled water. The ferrofluid was used to prepare a magnetic solution as a discontinuous phase. The final magnetic solution consists of poly(ethylene glycol)(700) diacrylate, (PEGDA, Polysciences), deionized water, and the ferrofluid (4 : 4 : 2 in volume) with 6% Darocur 1173 (v/v) and 0.5% Irgacure 819 (w/v) photoinitiators. Light mineral oil (Sigma) with 3% ABIL EM 90 (Degussa) (v/v) served as a continuous phase. The viscosity of the mineral oil was measured

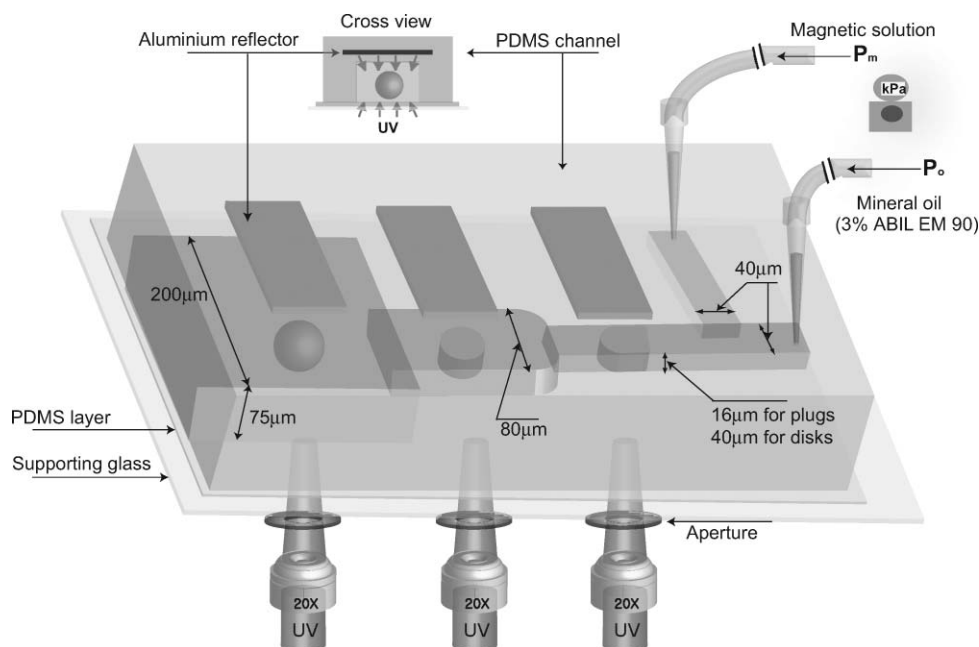


Fig. 1 Schematic diagram of the T-junction microfluidic channel with aluminium reflectors for spherical and non-spherical magnetic hydrogel synthesis: sphere, disk, and plug. P_m indicates the input pressure for the hydrogel precursors (dispersed phase) and P_o the input pressure for the mineral oil (continuous phase).

to be 0.03 Pa s at room temperature (297 K) using a Cannon-Manning Semi-Microviscometer (Cannon Instrument). The mineral oil solution was filtered using a 0.2 μm filter before use. The interfacial tension between the magnetic solution and the mineral oil was $4.23 \pm 0.23 \text{ mN m}^{-1}$ based on the pendant drop method using a DSA10 Tensiometer (Kruss).

2.3 Flow and UV-polymerization setup

The two immiscible fluids were independently driven into the PDMS channels by air pressure. Input pressures in the range of 0 to 103.4 kPa were controlled by a compressed air source ($\approx 275.8 \text{ kPa}$) using a type 100LR manual pressure regulator (Control Air) attached with a pressure gauge (DPG 100G, OMEGA). Average velocities of the continuous phase (the mineral oil) v_c were estimated as the velocity of plugs which fill the channel cross-section and move at a constant velocity v_p carried by the continuous phase, thus, $v_c \approx v_p$.^{40,41} A 100 W HBO mercury lamp served as the UV light source. The desired spectrum of UV light (with a maximum transmittance at 355 nm) from a wide UV spectrum was selected through a UV filter set (11000v2; UV, Chroma). The filtered UV light was exposed to targeted areas in the PDMS channels using a 20 \times microscope objective (Zeiss). The diameter (0–800 μm) of the UV-exposed area was controlled by an aperture in an inverted microscope (Axiovert 200, Zeiss). Formations of droplets and magnetic microhydrogels were visually observed using a CCD camera (KPM1A, Hitachi) mounted on the microscope and captured optical images were processed using NIH Image software. Diameters of sphere and disk magnetic microhydrogels and the long length of plug microhydrogels were measured based on captured optical images. A Nikon D200 camera (Digital SLR) was used to capture color images. Scanning electron microscopy (SEM, JEOLJSM 6060) was performed to obtain higher resolution images.

2.4 Magnetic characterization

To investigate the magnetic response of the particles, we examined their self-assembly in a PDMS reservoir in the presence of an external magnetic field. The reservoir ($\approx 2 \text{ mm} \times 2 \text{ mm} \times 4 \text{ mm}$) was fabricated by sealing a PDMS rectangular frame onto a PDMS-coated glass layer. The reservoir was then filled with spheres or plugs of the magnetic microhydrogels suspended in deionized water with 0.005% (v/v) Tergital NP-10. The reservoir was then placed in a uniform magnetic field (planar or normal) induced by an electromagnetic coil connected to a DC power supply (GPS-2303, GW Instek). The magnetic fields were calibrated using a Gauss meter (SYPRIS) with an axial probe for the normal induced magnetic field or a transverse probe for the planar induced field.

In addition to visually observing particle assembly, a vibrating sample magnetometer (VSM, Model 1660, ADE) was used to measure the magnetization of both magnetic nanoparticles and microhydrogels based on the dry mass. In VSM, an induced magnetization of the particles in a uniform magnetic field at a given strength is obtained from an electric field caused by oscillating the particles, and a full cycle of the magnetic fields (-0.5 T to 0.5 T) is applied to obtain their magnetization curve.

3 Results and discussion

3.1 Magnetic microhydrogel synthesis

The breakup of emulsion droplets in the T-junction of microfluidic devices can be characterized by: (i) capillary number $Ca = \mu v_c / \gamma$, which describes the competition between viscous and interfacial stresses where μ is the dynamic viscosity of the continuous phase, v_c is the flow velocity, and γ is the interfacial tension between the continuous and discontinuous fluids; (ii) the ratio of volumetric flow rates of the two phases, Q_c / Q_d ; and (iii) the geometric configuration of the junction: w_c , w_d , and h .^{25,42} The subscripts c and d indicate the continuous and discontinuous phases respectively. PDMS microfluidic devices have been well characterized in order to generate stable monodisperse emulsion droplets^{26,38,42,43} and to synthesize spherical and non-spherical microparticles in confined geometries of rectangular microchannels.^{30,31} In general, desired sizes of emulsion droplets are obtained by controlling either volumetric flow rates of two immiscible fluids, Q_c and Q_d , or applied pressures, P_c and P_d , depending on the experimental setup. A syringe pump is commonly used to impose constant Q_c and Q_d or a pressure regulator for P_c and P_d .^{25–27}

We initially employed the experimental setup shown in Fig. 1 to synthesize magnetic microhydrogels in the absence of the aluminium UV reflector. A desired diameter of spherical droplets was obtained by regulating P_c and P_d independently. In order to compensate for the strong UV absorption from the dispersed magnetic nanoparticles in the UV-curable PEG-base solution, we used a long UV exposure time, t_{UV} , which is determined by the velocity of a droplet traveling through a UV exposure area with a given diameter. However, regardless of the full curing of the spheres with $t_{UV} \approx 6 \text{ s}$, deformed spheres (*cf* Fig. 2a) were produced. Shape deformation occurred during the UV exposure. Currently, we do not have a detailed model to describe the failure to preserve the shape. However, we hypothesize that the deformation is attributed to two factors: (a) a non-uniform UV energy distribution along the surface of the emulsion droplets during the UV-curing because of the uni-directional UV exposure, and (b) a large gradient of UV energy along the direction of the light propagation within the droplets because of the strong UV absorption from the magnetic nanoparticles. In order to overcome the limitations of the polymerization scheme, a UV light reflector (aluminium foil) was introduced to the top of the channel as shown in Fig. 1. The aluminium reflector is expected to offer not only a multi-directional UV exposure to targeted magnetic emulsion droplets but is also expected to increase the net UV energy flux to the droplets, which allows for shorter exposure times.

The distance from the aluminium reflector to the top wall of the channel was found to be between 50 to 100 μm . To evaluate the effect of the aluminium reflector on the shape deformation, we repeated the previous experiment in the presence of the reflector except with higher P_0 and P_m applied to have a shorter t_{UV} . As expected, non-deformed spherical microhydrogels were successfully synthesized as shown in Fig. 2b. The required UV exposure time for the full polymerization was reduced to $t_{UV} \approx 4.3 \text{ s}$. This result implies that the aluminium reflector provides the expected polymerization conditions which prevent the shape deformation and reduce the UV exposure time. We also

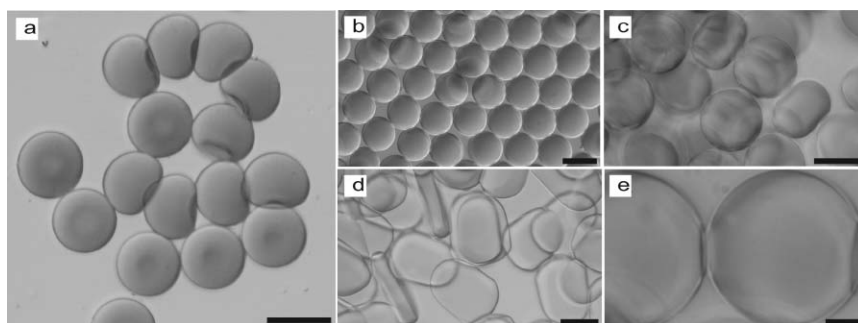


Fig. 2 Optical images of (a) deformed spherical magnetic microhydrogels in the absence of the aluminium UV reflector and (b)–(e) collections of magnetic microhydrogels in the presence of the aluminium UV reflector: (b) spheres, (c) disks, (d) plugs, and (e) high resolution of the disks. All particles are in mineral oil. Flow conditions for (a) the deformed spheres were $P_m = 20.7$ kPa, $P_o = 31.7$ kPa, and $Ca = 0.017$, (b) spheres: $P_m = 33.1$ kPa, $P_o = 52.4$ kPa, and $Ca = 0.029$, (c and e) disks: $P_m = 5.5$ kPa, $P_o = 12.4$ kPa, and $Ca = 0.016$, and (d) plugs: $P_m = 31.7$ kPa, $P_o = 46.9$ kPa, and $Ca = 0.023$. The scale bars are (a)–(d) 30 μm and (e) 10 μm .

implemented this polymerization scheme successfully to produce non-spherical magnetic hydrogels (disks and plugs) without any shape failure as shown in Fig. 2c for disks and Fig. 2d for plugs by confining spheres in different channel geometries as shown in Fig. 1. In the presence of the reflector, we were able to polymerize the disks and plugs within one second ($t_{UV} \approx 0.8$ s for the disks and $t_{UV} \approx 0.2$ s for the plugs), while at the same conditions but in the absence of the reflector, the droplets did not fully polymerize but relaxed back to spheres in the reservoir. Using the present method, we also show the ability to encapsulate magnetic nanoparticles uniformly in the polymer matrix as evidenced in the images shown in Fig. 2b–e. The disk shown in Fig. 2e exhibits no clusters of the magnetic nanoparticles within the microhydrogel. Furthermore, this enhanced polymerization scheme will be also highly effective in synthesizing various novel composite particles containing patterned internal microstructures such as magnetic hydrogels with aligned magnetic nanoparticles and hydrogels with liquid crystal textures. Rapid polymerization kinetics and homogeneous UV exposure are required in order to prevent clustering. In addition, the multi-directional UV exposure is essential to create core-shell structure particles such as hydrogel shells surrounding a core of a magnetic fluid. In the case of uni-directional UV exposure, the magnetic core would cast a circular shadow preventing the entire surface from being fully polymerized.

3.2 Morphology of the microhydrogels

Dried microhydrogels were used for SEM imaging after recovery from the continuous phase. Shown in Fig. 3a–c are SEM images of sphere, disk, and plug microhydrogels confirming preservation of the original polymerized shapes. This also demonstrates that the shapes are preserved during the volume shrinkage due to removal of water upon drying. In addition to their preserved shapes, they are highly monodisperse (coefficient of variation, CV is less than 2%) as shown in Fig. 3d–f. A sample with a CV of 5% or less is commonly accepted as being monodisperse.^{44,45} Measurements for CVs were performed using optical images of the microhydrogels collected in mineral oil after photopolymerization. Thus, the particles are hydrated and have dimensions larger than those in the SEM images.

By varying the dimensions of the T-junction, we were able to synthesize particles with various diameters as shown in Fig. 3a. For non-spherical microhydrogels, a taller channel with dimensions $h = 40$ $\mu\text{m}/w = 80$ μm was used to synthesize disks as shown in Fig. 3b and a short channel with dimensions $h = 16$ $\mu\text{m}/w = 40$ μm was used to synthesize thin plugs as shown in Fig. 3c. We were also able to obtain different lengths of the plugs by tuning the input pressures.

3.3 Magnetic characterization of the microhydrogels

3.3.1 Response to homogenous magnetic fields. Magnetic particles suspended in a non-magnetic medium exhibit various structural configurations arising from inter-particle interactions. In the presence of an external magnetic field, the magnetic particles acquire dipole moments and long-range dipolar interactions between the particles induce chain-like or columnar structures along the applied field direction.⁴⁶ Fig. 4 shows optical images of the self-assembly of magnetic microhydrogels when subject to uniform external magnetic fields. The resulting attractive interactions between the particles parallel to the field direction cause them to form long chains as shown in Fig. 4a and b. In contrast to spheres, disks and plugs exhibit a directional preference to an external magnetic field arising from their shape asymmetry. For instance, in Fig. 4c the plugs flip up perpendicular to the plane of view to align along the field direction. This unique magnetic response of anisotropic microparticles has great potential for many microscale applications. For instance, the field-induced pattern formed by magnetorheological fluids can operate as a sieving matrix in bio-chips^{47,48} and this application would benefit from the ability of anisotropic particles to form more complex patterns. Additionally, anisotropic magnetic particles could serve as rheological probes for microrheological characterization of complex fluids and biological materials⁴⁹ and also as basic components of portable microfluidic devices including field-responsive valves and mixers.⁵⁰ More importantly, biocompatibility, high surface area, and high target capturing capacity due to the porous structure⁵¹ of the non-spherical magnetic hydrogels will provide the advantages in biomedical applications including sorting and separation of biological materials,^{9,52,53} and immunoassays.¹⁰ However, to date, anisotropic magnetic

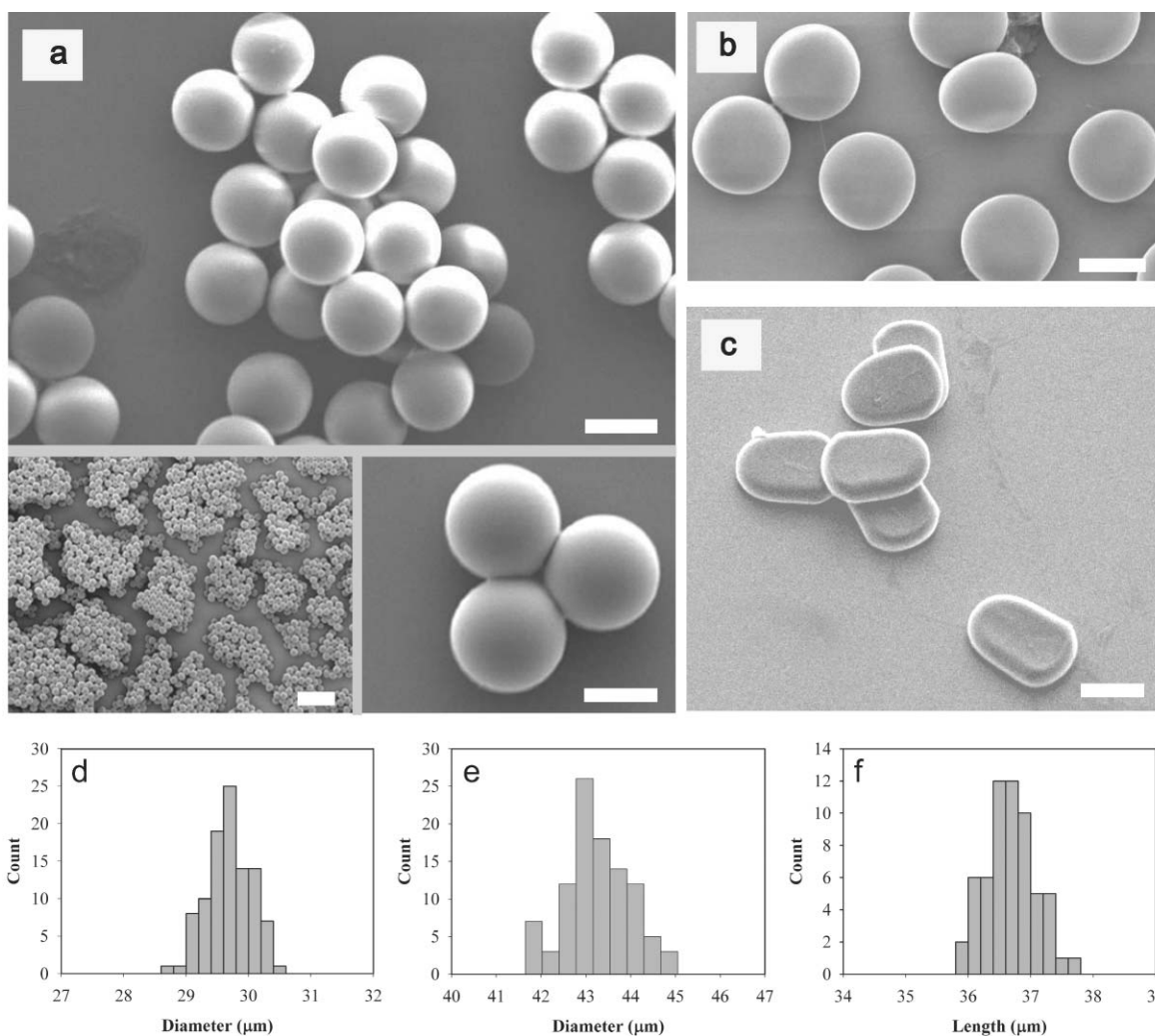


Fig. 3 SEM images of magnetic microhydrogels: (a) spheres, (b) disks, and (c) plugs, and distribution of the diameter of (d) the spheres [(a) top, coefficient of variation, CV = 1.2%], (e) the disks (CV = 1.6%), and (f) the long length of the plugs (CV = 1.3%). Flow conditions and channel dimensions of the T-junction for spheres were (a) top $P_m = 33.1$ kPa and $P_o = 52.4$ kPa with $h = 16$ $\mu\text{m}/w = 40$ μm , (a) bottom left $P_m = 50.3$ kPa and $P_o = 62.7$ kPa with $h = 20$ $\mu\text{m}/w = 15$ μm , and (a) bottom right $P_m = 49.0$ kPa and $P_o = 62.7$ kPa with $h = 10$ $\mu\text{m}/w = 15$ μm . In case of (b) disks and (c) plugs, $P_m = 5.5$ kPa and $P_o = 12.4$ kPa with $h = 40$ $\mu\text{m}/w = 40$ μm were applied for the disks and $P_m = 29.0$ kPa, $P_o = 46.9$ kPa with $h = 16$ $\mu\text{m}/w = 40$ μm were applied for the plugs. The scale bars are (a) top 20 μm , bottom left 50 μm , and bottom right 5 μm , and (b)–(c) 20 μm .

particles with uniform morphology and controlled size have not been realized and their availability could provide major benefits in these advanced applications.

3.3.2 Magnetic properties. Magnetic properties of the particles were measured using VSM. Fig. 5 shows the magnetization of two dried samples (a) magnetic nanoparticles and (b) spherical magnetic microhydrogels. Both magnetic nanoparticles and microhydrogels show superparamagnetic behavior and no hysteresis is found in a low field in either case. This is an important feature for practical use in bio-applications where no memory of magnetization after removing external magnetic fields is highly desirable.

Physical properties of the magnetic nanoparticles and microhydrogels are summarized in Table 1. All properties are based on the dry mass. The saturation magnetization for the nanoparticles and microhydrogels, M_{so} , and the mean diameter

of the nanoparticles, d (assuming the particles are spherical), can be obtained from the M – H curves (*cf* Fig. 5) using the following relation which is applicable at large fields:⁵⁴

$$M = M_{so} \left(1 - \frac{6}{\pi} \frac{k_b T}{M_s d^3 B} \right) \quad (1)$$

where M is the measured magnetization of the particles, k_b is the Boltzmann constant, T is the temperature (K), B is the magnetic field (T), and M_s is the saturation magnetization. For bulk maghemite, M_s values of 3.6×10^5 to 3.7×10^5 A m^{-1} ^{56,57} have been reported. We use $M_s = 3.7 \times 10^5$ A m^{-1} in eqn (1). We can determine M_{so} and d from the intercept and the slope of a linear fit of M versus $1/B$ at large values of B ($B = 0.2$ to 0.5 T). The computed diameter of the magnetic nanoparticles (6.8–7.6 nm) is within the typical range for maghemite nanoparticles (5 nm to 14 nm⁵⁸), while their M_{so} (64 $\text{A m}^2 \text{kg}^{-1}$) is smaller

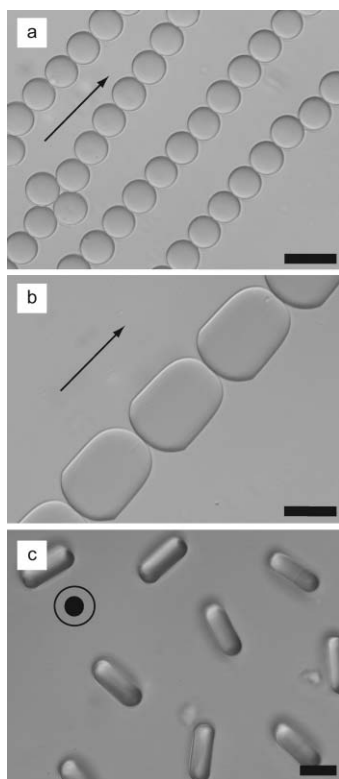


Fig. 4 Optical images showing self-assembly of (a) spheres and (b) and (c) plugs in response to homogeneous magnetic fields: (a) and (b) in-plane and (c) out-of-plane. Arrows indicate the field direction. The plugs exhibit a directional preference to the external applied field. Field strengths are: (a) and (b) 3.4 ± 0.17 mT and (c) 10.9 ± 0.48 mT. The spheres were produced at $P_m = 50.3$ kPa and $P_o = 62.7$ kPa with $h = 20 \mu\text{m}/w = 15 \mu\text{m}$ in the T-channel and plugs were produced at $P_m = 35.2$ kPa and $P_o = 53.4$ kPa with $h = 16 \mu\text{m}/w = 40 \mu\text{m}$. Scale bars are 25 μm .

than that for bulk maghemite ($76 \text{ A m}^2 \text{ kg}^{-1}$ ^{56,57}). The decrease in M_{so} relative to the bulk value is expected due to the presence of a magnetically disordered layer on the particle surface and a non-magnetic coated layer in order to avoid aggregation.^{15,58–60} The final magnetic nanoparticle content incorporated in the microhydrogels, 4.9%, is estimated from the initial composition

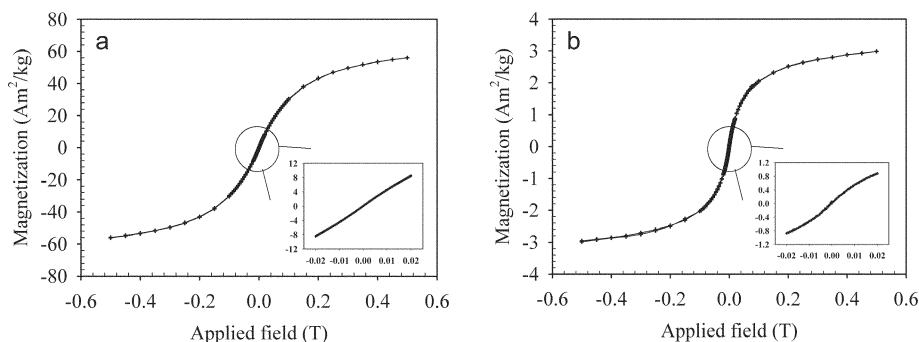


Fig. 5 $M-H$ curves of (a) dried nano-maghemite which is used in the present study to incorporate into the PEG-based polymer matrix and (b) dried magnetic microhydrogels (mean dried diameter 10.8 μm) containing the nano-maghemite using VSM. On the right bottom corner, the expanded magnetization curves in a lower applied field display no hysteresis. The microhydrogels were produced at $P_m = 50.3$ kPa and $P_o = 62.7$ kPa using $h = 20 \mu\text{m}/w = 15 \mu\text{m}$ in the T-channel. When solvated in water, the microhydrogels swell to have a diameter of 15 μm .

of the magnetic solution (assuming full conversion of PEGDA during the polymerization). We compare this estimated iron content to another estimation using the ratio of the values of M_{so} (*cf* Table 1) which gives an estimated mass fraction of 5.1%. The good agreement of these values leads us to conclude that the magnetic content in the hydrogel particles can be controlled by simply tuning initial compositions of magnetic prepolymer solutions, as anticipated. Finally, the initial magnetic susceptibilities, χ_{dry} , of the microhydrogels and nanoparticles were obtained from the slope of the $M-H$ curves at low applied fields. We note that χ_{dry} is based on the dry mass and thus has units $\text{m}^3 \text{ kg}^{-1}$.

The measured magnetic properties are inherently ensemble averages of a sample. To infer nanoparticle loading content in a single microparticle, we measured the optical absorption of spherical magnetic microhydrogels using grey scale images captured during the synthesis for two cases (diameters of 26 μm and 30 μm). Luminosity CVs (*cf* Fig. S1†) are less than 2% for both sets of particles, which shows that our method produces microhydrogels that have a very uniform loading of magnetic material.

Our method has several advantages when compared to bulk synthesis methods (*cf* Table S1†). Foremost, non-spherical particles can be produced in a continuous manner. Further, both particle size and magnetic loading per particle are very monodisperse. Only commercially produced magnetic particles are monodisperse; the other particles shown in Table S1† are polydisperse, based on the published optical images. Batch polymerization methods also face difficulties obtaining a homogenous distribution of inorganic particles incorporated into microgels.^{15,16} Our method can be easily extended to other types of monomers without compromising uniformity in the morphology and the distribution of embedded magnetic nanoparticles because processing parameters such as flow rates and channel geometry are uncoupled with initial and final physiochemical configurations of the composites. A current limitation of our technique is the modest magnetic loading; though this is comparable to some commercial beads (*e.g.* the COMPEL™ particles in Table S1†). Magnetic microhydrogels containing larger magnetic content can be obtained using our method through longer UV exposure (*e.g.* a long UV illuminated channel proving longer curing times³¹) or higher UV energy flux.

Table 1 Material properties of the magnetic nanoparticles and dried microhydrogels (MH)

	Diameter of nanoparticle/nm ^a	Diameter of MH/ μm	CV of MH diameter (%)	Iron ($\gamma\text{-Fe}_2\text{O}_3$) content wt (%)	Initial magnetic susceptibility $\chi_{\text{dry}}/\text{m}^3 \text{kg}^{-1}$	Saturation magnetization $M_{\text{so}}/\text{A m}^2 \text{kg}^{-1}$ ^a
Nanoparticle ($\gamma\text{-Fe}_2\text{O}_3$)	6.8				54×10^{-5}	64
Magnetic MH	7.6	10.8	1.5	4.9	8×10^{-5}	3.3

^a Estimated based the data from Fig. 5a and b using eqn (1).

4 Conclusions

A T-junction microfluidic device in combination with a UV light reflector has been developed to controllably synthesize magnetic hydrogel microparticles in spherical and non-spherical forms. The reflector mode approach has been shown to enhance UV-based polymerization conditions for the synthesis of the magnetic microhydrogels through an increased UV energy flux and a uniform distribution of UV energy. This enhanced polymerization scheme will significantly increase efficiency, even in general polymeric particle synthesis via UV-polymerization using microfluidic devices. More importantly, this method will be very effective and useful to generate various novel composite materials such as magnetic hydrogels patterned with aligned nano-magnetic particles, hydrogels patterned with liquid crystal textures, and magnetic hydrogel capsules.⁶¹

The magnetic hydrogel particles we synthesized exhibit superparamagnetic behavior, which is needed in most biological applications. In addition, non-spherical particles display an anisotropic response to an external magnetic field, which will offer beneficial features in various fundamental studies and applications. Future studies will be devoted to studying self-assembly and rheology of these model magnetic suspensions.

Acknowledgements

We gratefully acknowledge the support of NSF NIRT grant no. CTS-0304128 and the Singapore-MIT Alliance (SMA-II, CPE Program) for this project. We thank S. Vikram for his assistance with the VSM measurement. D. K. Hwang acknowledges the support from the Nature Science and Engineering Research Council of Canada (NSERC) for a postdoctoral fellowship.

References

- 1 M. J. Murray and M. J. Snowden, *Adv. Colloid Interface Sci.*, 1995, **54**, 73–91.
- 2 B. Lindlar, M. Boldt, S. Eiden-Assmann and G. Maret, *Adv. Mater.*, 2002, **14**, 1656–1658.
- 3 T. Nisisako, T. Torii and Y. Takizawa, *Adv. Mater.*, 2006, **18**, 1152–1156.
- 4 N. Pamme, *Lab Chip*, 2006, **6**, 24–38.
- 5 Q. A. Pankhurst, J. Connolly, S. K. Jones and J. Dobson, *J. Phys. D: Appl. Phys.*, 2003, **36**, R167–R181.
- 6 P. A. Voltairas, D. I. Fotiadis and L. K. Michalis, *J. Biomech.*, 2002, **35**, 813–821.
- 7 M. Hoehn, E. Kustermann, J. Blunk, D. Wiedermann, T. Trapp, S. Wecker, M. Focking, H. Arnold, J. Hescheler, B. K. Fleischmann, W. Schwindt and C. Buhle, *Proc. Natl. Acad. Sci. U. S. A.*, 2002, **99**, 16267–16272.
- 8 A. Jordan, R. Scholz, K. Maier-Hauff, M. Johannsen, P. Wust, J. Nadobny, H. Schirra, H. Schmidt, S. Deger, S. Loening, W. Lanksch and R. Felix, *J. Magn. Magn. Mater.*, 2001, **225**, 118–126.
- 9 M. Zborowski, L. R. Moore, P. S. Williams and J. J. Chalmers, *Sep. Sci. Technol.*, 2002, **37**, 3611–3633.
- 10 J. W. Choi, K. W. Oh, J. H. Thomas, W. R. Heineman, J. H. Nevin, A. J. Helmicki, H. T. Henderson and C. H. Ahn, *Lab Chip*, 2002, **2**, 27–30.
- 11 H. Kawaguchi, *Prog. Polym. Sci.*, 2000, **25**, 1171–1210.
- 12 V. Schmitt, F. Leal-Calderson and J. Bibette, *Top. Curr. Chem.*, 2003, **227**, 195–215.
- 13 K. Landfester, *Macromol. Rapid Commun.*, 2001, **22**, 896–936.
- 14 T. Fujibayashi and M. Okubo, *Langmuir*, 2007, **23**, 7958–7962.
- 15 C. Menager, O. Sandre, J. Mangili and V. Cabuil, *Polymer*, 2004, **45**, 2475–2481.
- 16 K. Landfester and L. P. Ramirez, *J. Phys.: Condens. Matter*, 2003, **15**, sl345–sl361.
- 17 E. Matijevic, *Langmuir*, 1994, **10**, 8–16.
- 18 H. Yu, M. Chen, P. M. Rice, S. X. Wang, R. L. White and S. H. Sun, *Nano Lett.*, 2005, **5**, 379–382.
- 19 Y. Yin and Y. Xia, *Adv. Mater.*, 2001, **13**, 267–271.
- 20 V. N. Manoharan, M. T. Elsesser and D. J. Pine, *Science*, 2003, **301**, 483–487.
- 21 D. Dendukuri, D. C. Pregibon, J. Collins, T. A. Hatton and P. S. Doyle, *Nat. Mater.*, 2006, **5**, 365–369.
- 22 J. P. Rolland, B. W. Maynor, L. E. Euliss, A. E. Exner, G. M. Denison and J. M. De Simone, *J. Am. Chem. Soc.*, 2005, **127**, 10096–10100.
- 23 J. A. Champion, Y. K. Katare and S. Mitragotri, *Proc. Natl. Acad. Sci. U. S. A.*, 2007, **104**, 11901–11904.
- 24 J. W. Kim, R. J. Larsen and D. A. Weitz, *J. Am. Chem. Soc.*, 2006, **128**, 14374–14377.
- 25 G. F. Christopher and S. L. Anna, *J. Phys. D: Appl. Phys.*, 2007, **40**, R319–R336.
- 26 T. Thorsen, R. W. Roberts, F. H. Arnold and S. R. Quake, *Phys. Rev. Lett.*, 2001, **86**, 4163–4166.
- 27 S. L. Anna, N. Bontoux and H. A. Stone, *Appl. Phys. Lett.*, 2003, **82**, 364–366.
- 28 P. Garstecki, I. Gitlin, W. Diluzio, G. M. Whitesides, E. Kumacheva and H. A. Stone, *Appl. Phys. Lett.*, 2004, **85**, 2649–2651.
- 29 P. Garstecki, H. A. Stone and G. M. Whitesides, *Phys. Rev. Lett.*, 2005, **94**, 164501.
- 30 D. Dendukuri, K. Tsoi, T. A. Hatton and P. S. Doyle, *Langmuir*, 2005, **21**, 2113–2116.
- 31 S. Xu, Z. Nie, M. Seo, P. Lewis, E. Kumacheva, H. A. Stone, P. Garstecki, D. B. Weibel, I. Gitlin and G. M. Whitesides, *Angew. Chem., Int. Ed.*, 2005, **44**, 724–728.
- 32 B. G. De Geest, J. P. Urbanski, T. Thorsen, J. Demeester and S. C. De Semdt, *Langmuir*, 2005, **21**, 10275–10279.
- 33 M. Seo, Z. H. Nie, S. Q. Xu, P. C. Lewis and E. Kumacheva, *Langmuir*, 2005, **21**, 4773–4775.
- 34 W. J. Jeong, J. Y. Kim, J. B. Choo, E. K. Lee, C. S. Han, D. J. Beebe, G. H. Seong and S. H. Lee, *Langmuir*, 2005, **21**, 3738–3741.
- 35 R. F. Shepherd, J. C. Conrad, S. K. Rhodes, D. R. Link, M. Marquez, D. A. Weitz and J. A. Lewis, *Langmuir*, 2006, **22**, 8618–8622.
- 36 T. Nisisako, T. Torii and T. Higuchi, *Chem. Eng. J.*, 2004, **101**, 23–29.
- 37 J. W. Kim, A. S. Utada, A. Fernandez-Nieves, Z. B. Hu and D. A. Weitz, *Angew. Chem., Int. Ed.*, 2007, **46**, 1819–1822.
- 38 J. D. Tice, A. D. Lyon and R. F. Ismagilov, *Anal. Chim. Acta*, 2004, **507**, 73–77.
- 39 R. Massart, *Fr. Pat.* 2461521, 1981; R. Massart, S. Neveu, V. Cabuil-Marchal, R. Broussel, J. M. Fruchart, T. Bouchami, J. Roger, A. Bee-Debras, J. N. Pons and M. Carpentier, *Fr. Pat.* 2662539, 1991.
- 40 H. A. Stone, A. D. Stroock and A. Ajdari, *Annu. Rev. Fluid Mech.*, 2004, **36**, 381–411.

-
- 41 T. Ward, M. Faivre, M. Abkarian and H. A. Stone, *Electrophoresis*, 2005, **26**, 3716–3724.
- 42 P. Garstecki, M. J. Fuerstman, H. A. Stone and G. M. Whitesides, *Lab Chip*, 2006, **6**, 437–446.
- 43 J. H. Xu, G. S. Luo and G. G. Chen, *Lab Chip*, 2006, **6**, 131–136.
- 44 A. Jillavenkatesa, S. J. Dapkunasand L. H. Lum, Particle Size Characterization Technical Report, *Journal of Research of the National Institute of Standards and Technology*, NIST, Gaithersburg, MD, USA, 2001, pp. 960–961.
- 45 S. Takeuchi, P. Garstecki, D. B. Weibel and G. M. Whitesides, *Adv. Mater.*, 2005, **17**, 1067–1072.
- 46 R. E. Rosensweig, *Ferrohydrodynamics*, Cambridge University Press, New York, 1985.
- 47 P. S. Doyle, J. Bibette, A. Bancaud and J. L. Viovy, *Science*, 2002, **295**, 2237–2237.
- 48 N. Mine, P. Bokov, K. B. Zeldovich, C. Futterer, J. L. Viovy and K. D. Dorfman, *Electrophoresis*, 2005, **26**, 362–375.
- 49 A. S. Khair and J. F. Brady, *J. Rheol.*, 2008, **52**, 165–196.
- 50 A. K. Vuppu, A. A. Garcia and M. A. Hayes, *Langmuir*, 2003, **19**, 8646–8653.
- 51 D. C. Pregibon, M. Toner and P. S. Doyle, *Science*, 2007, **315**, 1393–1396.
- 52 D. W. Inglis, R. Riehn, R. H. Austin and J. C. Sturm, *Appl. Phys. Lett.*, 2004, **85**, 5093–5095.
- 53 N. Xia, T. P. Hunt, B. T. Mayers, E. Alsberg, G. M. Whitesides, R. M. Westervelt and D. E. Ingber, *Biomed. Microdevices*, 2006, **8**, 299–308.
- 54 G. Fønnum, C. Johansson, A. Molteberg, S. Morup and E. Aksnes, *J. Magn. Magn. Mater.*, 2005, **293**, 41–47.
- 55 G. Bate, *Ferromagnetic Materials*, vol. 2, North-Holland Publishing Company, New York, 1980.
- 56 B. D. Cullity, *Introduction to Magnetic Materials*, Addison-Wesley Publishing Company, Reading, MA, 1972.
- 57 P. Weiss and R. Forrer, *Ann. Phys.*, 1929, **12**, 279.
- 58 J. C. Bacri, R. Perzynski, D. Salin, V. Cabuil and R. Massart, *J. Magn. Magn. Mater.*, 1986, **62**, 36–46.
- 59 A. Millan, A. Urtizberea, N. J. O. Silva, F. Palacio, V. S. Amaral, E. Snoeck and V. Serin, *J. Magn. Magn. Mater.*, 2007, **312**, L5–L9.
- 60 Z. Shan, W. S. Yang, X. Zhang, Q. M. Huang and H. Ye, *J. Braz. Chem. Soc.*, 2007, **18**, 1329–1335.
- 61 H. Y. Koo, S. T. Chang, W. S. Choi, J. H. Park, D. Y. Kim and O. D. Velev, *Chem. Mater.*, 2006, **18**, 3308–3313.